

Precision at Scale: Domain-Specific Datasets On-Demand

Jesús M Rodríguez-de-Vera^{*1}, Imanol G Estepa^{*1}, Ignacio Sarasúa²,
Bhalaji Nagarajan¹, and Petia Radeva¹

¹ Universitat de Barcelona, Spain

j.molina.rdv@ub.edu, igonzaes42@alumnes.ub.edu, bhalaji.nagarajan@ub.edu,
petia.ivanova@ub.edu

² NVIDIA Corporation, Spain
isarasua@nvidia.com

Abstract. In the realm of self-supervised learning (SSL), conventional wisdom has gravitated towards the utility of massive, general domain datasets for pretraining robust backbones. In this paper, we challenge this idea by exploring if it is possible to bridge the scale between general-domain datasets and (traditionally smaller) domain-specific datasets to reduce the current performance gap. More specifically, we propose *Precision at Scale* (PaS), a novel method for the autonomous creation of domain-specific datasets on-demand. The modularity of the PaS pipeline enables leveraging state-of-the-art foundational and generative models to create a collection of images of any given size belonging to any given domain with minimal human intervention. Extensive analysis in two complex domains, proves the superiority of PaS datasets over existing traditional domain-specific datasets in terms of diversity, scale, and effectiveness in training visual transformers and convolutional neural networks. Most notably, we prove that automatically generated domain-specific datasets lead to better pretraining than large-scale supervised datasets such as ImageNet-1k and ImageNet-21k. Concretely, models trained on domain-specific datasets constructed by PaS pipeline, beat ImageNet-1k pretrained backbones by at least 12% in all the considered domains and classification tasks and lead to better food domain performance than supervised ImageNet-21k pretrain while being 12 times smaller. Code repository: <https://github.com/jesusmolrdv/Precision-at-Scale/>

Keywords: Dataset creation · Domain-specific data · SSL

1 Introduction

Recently, big transformer models have been dominating over the state-of-the-art. Works such as DINOv2 [50], when trained on millions of images in a completely self-supervised way, manage to obtain very high performance on most of the general discriminative tasks. However, as most of these models focus on being as

* Equal contribution

general as possible, they require a huge amount of general images to provide high performance on domain-specific tasks. Usually, these images are provided in the form of an unsupervised or programatically created dataset we call pretrainer dataset or just pretrainer. If the difficulty of the target domain increases, it is harder for these pretrainers to provide the required richness and diversity to the trained models, as they do not focus on any particular domain at all.

Different works, acknowledging this problem, propose domain-specific datasets that aim to train domain expert models [6,45,46]. While supervised and domain-specific, these datasets require expensive investments in human domain experts who label them. For this reason, most of them contain a small number of images compared to the popular unsupervised datasets [50,57], which makes them a worse option for current SoTA architectures [18]. So, even if domain-specific datasets prove to be better than general ones in their own expertise, they lack the scalability required nowadays. Lately, image generation and synthetic dataset generation have started to gain strength, proving to be comparable to real datasets [26,61] and being able to provide dataset scalability *on demand*. SynCLR [61], for example, leverages the use of an initial set of general captions extracted from a supervised dataset to create a completely synthetic dataset. Nevertheless, the use of real labels still constraints the approach by introducing an external "supervision".

In our work, we study the possibility of constructing completely on-demand domain-specific datasets and analyse their capacities as pretrainers for ViTs. Accordingly, we propose a multi-stage pipeline, which we call PaS, that does not have human dependence such as external labels or experts. By leveraging current SoTA Image Generation models [54] and huge unsupervised datasets [57], we are able to create and curate domain-specific datasets (defined as PaS datasets) on-demand that prove to be better pretrainers than general datasets such as ImageNet-1k [55]. Regarding current SoTA domain-specific datasets [6,46,63,66], we analyse the diversity and compare it with our PaS datasets, showing how PaS is perfectly able to match the diversity of human-created datasets while providing much bigger datasets. In summary, the contributions of this paper are: **1) We propose PaS, a domain-specific dataset creation pipeline that given a domain creates a hybrid synthetic and real dataset at a given scale. 2) Our PaS datasets provide more diversity than current SoTA domain-specific datasets without any drawback and our extensive analysis of two different domains proves that PaS datasets are much better pretrainers, outperforming popular datasets by more than 10% on classification tasks. 3) At the same scale, models trained in our PaS datasets surpass models trained in current domain-specific datasets across domains, evaluation datasets and downstream tasks. When compared to ImageNet-1k, PaS datasets demonstrate that on the same or even smaller scale, domain-specific datasets beat general ones on multiple downstream tasks and domains, proving that quality stands over quantity on model pretrain setups. 4) PaS datasets prove to be beneficial for different CNN sizes, enhancing their performance by more than 3% on linear probing and 0.3% on fine-tune settings.**

2 Related Works

Unsupervised Dataset Generation. Given the high demand for data, shown by recent models [69, 77] the creation of datasets at scale has started to be a priority task. Big unsupervised datasets such as LAION-2B [57] enable the use of custom subsets adapted to each use case and model. Recent papers like DINOv2 [50] and Internet Explorer [37] propose automatic pipelines to retrieve and curate real images and compose a more sophisticated dataset that includes high-quality samples while being completely unsupervised. Recently, the success of generative models such as Stable Diffusion [54] and MUSE [8] encouraged works that propose the creation of a completely synthetic dataset [3]. SynCLR [61] leverages the available labels in SoTA datasets to create a completely synthetic dataset of 600 million images and 150 million captions. Similarly, SynthCLIP [26] creates synthetic image-text pairs at scale by exploiting the knowledge of a previously created Meta-CLIP’s concept bank.

Self-supervised Model Pretraining in Deep learning: ImageNet-trained [55] models have been widely used as initialization weights across diverse downstream tasks such as classification, localization, and segmentation [76]. Model pretraining reduces the need for extensive task-specific datasets [36]. However, models such as ConvNext [69], ViT-G [77] and ViT-22B [15] demand substantial training data, often sourced from ImageNet-22K [16], or JFT [77]. Self-supervised learning (SSL) enables models to acquire adaptable generic features aligned with the original trained model [2, 10, 22, 25, 28]. These models, designed to generate visual features, work effortlessly on any image and pixel-level task [50]. Their success owes to the surge in computational power, model complexity, and data scale by orders of magnitude [13]. BEiT [4], MAE [27] and SimMIM [73] are achieving more and more popularity due to their capacity to contribute to creating robust and efficient models capable of learning in a self-supervised way. A very recent trend focuses on creating task-specific models such as SAM [35] for segmentation and OWL-ViT [47] for detection.

Vision-Language Models (VLM): VLMs like CLIP [53], ALIGN [31], and BASIC [51] play a crucial role in the success of pretrained models. Dual-encoder models [31, 53] learn context-aware representations from both text and visual contents in the shared latent space [21, 38, 80]. VLMs thus provide zero-shot image manipulations guided by textual prompts [23, 34, 59, 79]. Encoder-decoder architectures [68] like CoCa [76] and ImageBind [24] learn generic representations across different modalities. BLIP-2 [39] uses frozen image encoders and LLMs to enhance performance across various vision tasks. Flamingo [1] and Florence-2 [71] are large VLMs demonstrating capabilities in comprehensive vision tasks. A significant bottleneck in VLMs is the need for extensively aligned text-image corpora. Recent endeavours exploring weakly-supervised approaches, like hashtag-supervision, could result in a noisy corpus [30, 42]. Additionally, their utility is limited by the lack of pixel-level information [50]. Furthermore, it is noteworthy that several corpora, including ALIGN-1.8B [31], and FLD-5B [71] are not publicly released, posing significant obstacles for the research community.

3 PaS: Dataset Construction Pipeline On-Demand

In this section, we introduce Precision at Scale (PaS), a novel method aimed at generating on-demand domain-specific datasets with minimal human intervention. The essence of PaS lies in its completely autonomous workflow, which begins with the leverage of large language models (LLMs) for the discovery of domain-specific concepts. This first stage sets the groundwork by identifying a broad bank of relevant concepts (Section 3.1). Following the concept discovery, the method embarks on a second stage that collects real images and generates synthetic images corresponding to these concepts. The dual approach not only enriches the dataset with a wide variety of real-world images, but also enhances it with synthetic images covering a broader aspect of the concepts (Section 3.2). Finally, the workflow refines the dataset by applying advanced curation techniques eliminating redundancies and filtering out irrelevant or out-of-domain content (Section 3.3). Ultimately, the method yields a highly precise dataset that is primed for training visual models in a self-supervised manner as well as scaled according to the resources and use case of the target models. The modularity of PaS is one of its core traits: note that we do not make assumptions in the specific LLMs, image generators, or image sources used.

3.1 Stage 1: In-domain LLM-guided Concept Discovery

The first stage of our pipeline consists of the acquisition of an extensive bank of concepts, \mathcal{B} , belonging to the domain \mathcal{D} . Despite its vast collection of 500.000 concepts, the MetaCLIP concept repository [74] fails to provide extensive coverage in certain specific domains (e.g. in the Mediterranean food domain, it “only” contains simple *paella* as concept, disregarding all the common variations of it). In order to build $\mathcal{B} \subset \mathcal{D}$ without human expert supervision, we leverage the knowledge embedded in Large Language Models (LLM). To guide the LLM, it is necessary to textually define \mathcal{D} . To limit the biases introduced during the generation process, we reduce this process to two text strings that will be used in the LLM prompts: the name of the domain, $n_{\mathcal{D}}$, and a short description of the type of concepts that make up the domain, $d_{\mathcal{D}}$. For example, if \mathcal{D} is the domain of all species of birds in the world, we could define $n_{\mathcal{D}} = \text{“birds”}$ and $d_{\mathcal{D}} = \text{“bird species”}$. The process to generate \mathcal{B} involves three guided functions by any LLM: 1) generation, 2) expansion, and 3) filtering.

Generation of an initial set of concepts: Different to other approaches, we do not use a previously curated list of concepts to build \mathcal{B} . Thus, we first need to create an initial set \mathcal{B}_0 which should be task-agnostic while being domain-specific in order to properly cover the target domain. To achieve this, we leverage a LLM, L_1 , which we provide only with $n_{\mathcal{D}}$ and $d_{\mathcal{D}}$. In particular, we use the first prompt template displayed in Figure 1 to query L_1 . LLMs are stochastic by nature unless a random seed is fixed at inference time. Given that different random seeds might lead to different (potentially incomplete) outputs, we consider from now on the output of the used LLMs as a probability distribution. In this way, let $G_{L_1}(n_{\mathcal{D}}, d_{\mathcal{D}})$ denote the probability distribution over sets of concepts

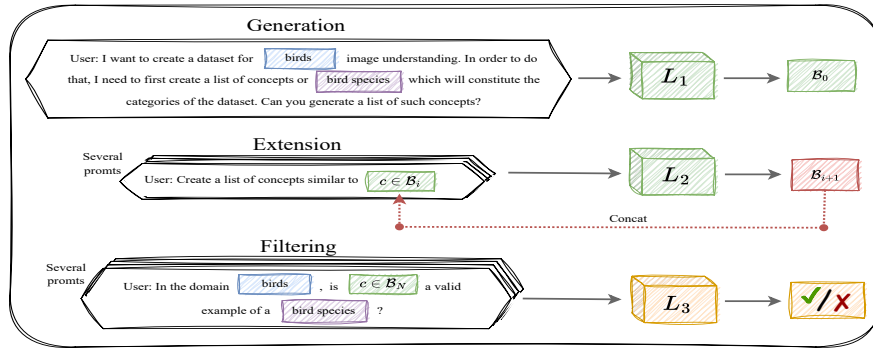


Fig. 1: Stage 1 workflow. Based on the output concepts of an initial prompt, we extend the output by chaining N number of prompts. Once we saturate the diversity, we filter them using by prompting an auxiliary LLM.

generated by L when prompted. Due to the reduced guidance, the first generated text by the model can induce a bias. To mitigate this, we introduce a strategy that diversifies the concept generation by sampling G_{L_1} using different random seeds. This aggregation forms a collective set \mathcal{C}_N , which is composed of concepts generated across N iterations, each with its unique seed.

We continue sampling and expanding \mathcal{C}_N until the addition of new concepts ceases to significantly augment the diversity of the set. Specifically, we stop when the difference between the size of the new set of concepts \mathcal{C}_N and the previous set \mathcal{C}_{N-1} is less than a predetermined fraction λ_1 of \mathcal{C}_{N-1} 's size: $(\mathcal{C}_N \setminus \mathcal{C}_{N-1}) < \lambda_1 \cdot |\mathcal{C}_{N-1}|$, where $\lambda_1 \in (0, 1)$ is a hyper-parameter that we set empirically. This criterion ensures we strike a balance between exploring a wide range of concepts and maintaining generational efficiency. The resulting initial concept bank \mathcal{B}_0 is thus a consolidated collection of all concepts up to \mathcal{C}_N , providing a comprehensive foundation for further refinement and exploration specific to the domain. For instance, in the domain of birds, the initial concepts might include a variety of species such as **Canada Goose**, **Crow**, and **Imperial Eagle**.

Domain Exploration via Concept Expansion: The second step involves enriching the concept bank within domain \mathcal{D} . The initial set of relevant concepts, \mathcal{B}_0 , can be further refined iteratively by a LLM, denoted as L_2 , which may or may not be the same as L_1 . To this end, we prompt L_2 to generate similar concepts for every c already in the concept bank. We define as $E_{L_2}(n_{\mathcal{D}}, d_{\mathcal{D}}, \mathcal{B}_i, c)$ the probability distribution generated by L_2 when asked to generate similar concepts to c using the second template in Figure 1. To provide more context to L_2 , the conversation with L_1 to generate \mathcal{B}_0 is used as historic data. By explicitly asking L_2 for concepts similar to the existing ones, we guide the model to populate the domain with concepts that are closely aligned with the established set. Formally, the iterative process is $\mathcal{B}_{i+1} = \mathcal{B}_i \cup \bigcup_{c \in \mathcal{B}_i} \{e_{\mathcal{D},c} \sim E_{L_2}(n_{\mathcal{D}}, d_{\mathcal{D}}, \mathcal{B}_i, c)\}$. To manage this expansion efficiently, we apply a stopping criterion similar to that of the initial generation phase: expansion ceases when $(\mathcal{B}_{i+1} \setminus \mathcal{B}_i) < \lambda_2 \cdot |\mathcal{B}_i|$. Again,

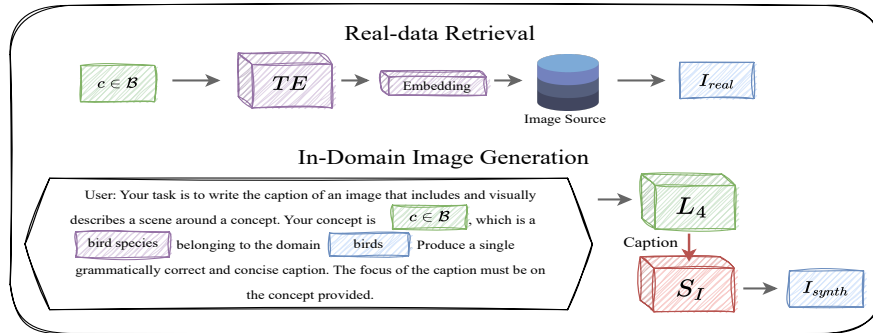


Fig. 2: Stage 2 Workflow. For every valid concept extracted on the first stage, we collect the most N similar images from a real-data source. Similarly, we prompt an image generation algorithm using the concept to produce a set of synthetic images. The combination of both sets form the unfiltered version of the desired dataset.

$\lambda_2 \in (0, 1)$ is an empirically set hyper-parameter. For example, when asked to expand the concept **Imperial Eagle**, a potential answer of L_3 would include elements like **Bald Eagle**, **Harpy Eagle**, **Crested Eagle** or **Golden Eagle**.

Concept filtering: LLMs are prone to hallucinate [48]. Since \mathcal{B} is the starting point for the rest of the pipeline, it is important to reduce the number of concepts in $\mathcal{B} \setminus \mathcal{D}$ (concepts generated that do not belong to the target domain). To this end, we use an additional LLM, L_3 , to validate each one of the concepts generated by L_1 . By setting $L_1 \neq L_3$, we can use it as a regulatory mechanism, since the differences in architecture and weights would mitigate the likelihood of both LLMs making a mistake in the same concept. Using the third template displayed in Figure 1, $V_{L_3}(n_{\mathcal{D}}, d_{\mathcal{D}}, c)$ represents the decision³ of L_3 about whether or not the concept c belongs to \mathcal{D} . Only concepts validated by L_3 are retained in the final bank of concepts $\mathcal{B} = \left\{ c \in \bigcup_{i=0}^N \mathcal{B}_i : V_{L_3}(n_{\mathcal{D}}, d_{\mathcal{D}}, c) = \text{True} \right\}$.

3.2 Stage 2: Collecting Domain-Specific Images

Uncurated Real-Data Retrieval: In this stage, we aim to compile domain-specific real-world images leveraging our concept bank \mathcal{B} . For each concept c , we generate a textual embedding, $\mathbf{t}_c = TE(c)$, where $TE(\cdot)$ is the text encoder of a chosen vision-language model. This model provides a unified embedding space for both text and images, enabling direct comparison with visual data. We search an extensive index of uncurated images, employing the same vision-language model’s visual encoder, $VE(\cdot)$, to compute the visual embeddings $\mathbf{v}_I = VE(I)$ for each image. The selection of images is based on the cosine similarity $\text{sim}(\mathbf{t}_c, \mathbf{v}_I) = \frac{\mathbf{t}_c \cdot \mathbf{v}_I}{\|\mathbf{t}_c\| \|\mathbf{v}_I\|}$ between the concept’s textual embedding and the image’s visual embedding, ensuring a high degree of relevance to \mathcal{D} . This process produces \mathcal{I}_{real} , a dataset of real images closely aligned with \mathcal{B} .

³ We consider a single output of L_3 with a fixed random seed.

In-Context In-Domain Image Generation: The initial phase in the creation of synthetic images involves the **generation of textual prompts**. Contrary to direct methods that might employ the plain name of a concept (e.g. **Canada Goose**) for image generation, our approach adopts a more nuanced strategy. We use a LLM, denoted as L_4 , to craft detailed image captions that encapsulate the essence of a given concept $c \in \mathcal{B}$. This is achieved by employing a structured template, as illustrated in Figure 2, which guides the LLM towards producing rich, contextually relevant captions. The probability distribution of captions by L_4 for concept c is represented as $P_{L_4}(c)$. We sample N_{Cap} captions for each concept, $\mathcal{T}_c = \{t_c \sim P_{L_4}(c)\}$, creating scene descriptions that enrich the conceptual depiction, (e.g. "A majestic **Canada Goose** spreads its wings, taking flight above the frozen lake."). These captions are then provided to a text-to-image model (e.g. Stable Diffusion [54]), S_I , which creates N_{Synth} synthetic images for each caption: $\mathcal{I}_{Synth} = \bigcup_{c \in \mathcal{B}} \bigcup_{t \in \mathcal{T}_c} \{i_t \sim S_I(t)\}$. The template for L_4 is designed to ensure captions contextualize the concept within a scene, improving the descriptive quality and diversity of the synthetic images. The parameters N_{Cap} and N_{Synth} are adjustable to control the volume and variety of \mathcal{I}_{Synth} . The final set of images, composed by both real and synthetic images, is denoted as $\mathcal{I} = \mathcal{I}_{Real} \cup \mathcal{I}_{Synth}$.

3.3 Stage 3: Dataset Curation

This stage focuses on refining \mathcal{I} , the dataset assembled in Stage 2, to enhance its quality and relevance for domain \mathcal{D} . By eliminating low-quality and out-of-distribution (OOD) images, we reduce training costs and prevent the potential negative impact on model performance.

Self-Supervised Similarity-based Removal: Duplicate and closely similar images increase the image count (and resource consumption) without adding to the diversity of the data. We employ Self Supervised Copy Detection (SSCD) [52] to identify and remove such instances. Each image I_i in \mathcal{I} is transformed into a latent representation through the visual encoder of SSCD, denoted as $VE_{SSCD}(I_i)$. We then construct an adjacency matrix A , where $A_{ij} = 1$ if the cosine similarity between $VE_{SSCD}(I_i)$ and $VE_{SSCD}(I_j)$ is above a predefined threshold λ_{dup} . From each connected component in A , we retain only one image (randomly selected), effectively reducing redundancy.

CLIP-based OOD Assessment: Given that \mathcal{I} is partially sourced from uncurated sources and generated using unsupervised methods, it may contain OOD images. To address this, we employ the zero-shot capabilities of CLIP [53]. Recent works like CLIPN [21] enhance the ability of OOD detection with CLIP by learning *negative prompts*. These prompts guide the model to learn what the concept *is not*, improving its discrimination capability. This dual-prompt approach allows CLIPN to calculate two probabilities for each image I and concept c : $p_{c,I}$, the likelihood that I contains a concept c , and $p_{c,I}^{no}$, the likelihood that I does not contain c . These probabilities are used to compute the OOD score for I with respect to the concept bank \mathcal{B} : $OOD_{\mathcal{B}}(I) = 1 - \sum_{c \in \mathcal{B}} (1 - p_{c,I}^{no}) \cdot p_{c,I}$.

We evaluate the OOD status of an image I using three metrics: $\text{OOD}_{\mathcal{B}}(I)$, $\text{OOD}_{\mathcal{B}'}(I)$ for a generalized concept set \mathcal{B}' , and $\text{OOD}_{\mathcal{B}}(I') - \text{OOD}_{\mathcal{B}}(I)$, where I' is a variant of I with text regions blurred. Particularly, a text-detection algorithm is used to find the text present in every image. This approach aims to reduce biases in the CLIP score introduced by the textual content in the images [43], focusing the OOD evaluation on the visual content.

Pareto Front-based Removal: Based on those three metrics, a Pareto-front method for multi-objective optimization [49] is utilized for image selection, where an image I is considered less suitable than the image J (and therefore prioritized for removal) if it shows higher OOD scores across the metrics: $\text{OOD}_{\mathcal{B}}(I) \geq \text{OOD}_{\mathcal{B}}(J)$, $\text{OOD}_{\mathcal{B}'}(I) \geq \text{OOD}_{\mathcal{B}'}(J)$, $\text{OOD}_{\mathcal{B}}(I') - \text{OOD}_{\mathcal{B}}(I) \geq \text{OOD}_{\mathcal{B}}(J') - \text{OOD}_{\mathcal{B}}(J)$; with at least one metric showing a strict increase. This approach ensures the systematic exclusion of images that are less relevant for our dataset, enhancing the dataset’s overall quality and relevance to the target domain. To determine the optimal stopping point for this pruning process, we employ the kneedle algorithm [56]. This algorithm identifies the "knee" point on a curve that represents the relationship between the average value of each metric at the i -th Pareto-front (Y-axis) and the cumulative number of images removed up to that point (X-axis). By selecting the maximum X value among the three knees (one per metric), we can estimate the most efficient halt point. This balance ensures that we maximize the improvement in OOD metric performance while minimizing the loss of potentially valuable images. Furthermore, in addition to this heuristic stopping criteria, the Pareto optimization process also provides a structured guidance for filtering the dataset down to any desired size, offering a flexible approach to achieve a tailored dataset size.

3.4 Stage 4: Data Usage

The culmination of Stage 3 is a meticulously curated, domain-specific dataset, assembled autonomously without human oversight. While the collection process is driven by specific concepts, the lack of supervision could introduce some noise in the concept-image correlations. Because of this, among the potential applications for the datasets produced by PaS, we highlight training SSL models as a particularly fitting use case. These approaches are known for their demand for large and diverse datasets, making them ideal candidates for utilizing our generated datasets (since PaS can generate an arbitrary amount of samples). Consequently, we employ the generated dataset to train a visual backbone in a self-supervised manner. This pretrained backbone can subsequently be adapted to various downstream tasks within the domain, showcasing the broad applicability and potential of datasets created by our framework.

4 Experiments

In this section, we evaluate the proposed methodology in two different and complex domains: bird species and food. First, we analyse the diversity and domain

alignment of the generated datasets and the largest manually curated datasets for each domain by comparing their lexical and image distributions. Secondly, we evaluate the transferability of the features learned using the generated datasets in a variety of downstream tasks of each domain. Finally, we compare the performance obtained when pretraining in large-scale general domain datasets and that achieved by the models pretrained with PaS datasets.

4.1 Experimental Setup

Domains: *Birds* and *food* have attracted the attention of the computer vision community due to their fine-grained nature and the existence of widely adopted benchmarks for different computer vision tasks. In the *birds* domain, we consider three existing supervised datasets: CUB-200-2011 [66], NABirds [63] and the subset of bird species of iNat-2021 [64] (iNat_{birds} from now on). Regarding *food*, we consider also three existing and widely used datasets: Food-101 [6], FoodX-251 [33] and the current state-of-the-art food dataset Food-2K [46].

Dataset generation: For Stage 1 of the generation of the data set, we used as $L_1 = L_2$ the open LLM Mixtral-8x7B [32], and as L_3 Llama 2-13B [62]. We set $\lambda_1 = \lambda_2 = 0.01$ resulting in \mathcal{B}_{food} (5K concepts) and \mathcal{B}_{birds} (3K concepts). In Stage 2, we use LAION-5B [57] as the source of uncurated real images. We sample 500 images per concept using OpenAI’s CLIP ViT-L/14 [53] to build the image index and the text embeddings. We use Stable Diffusion 2.1 (SD 2.1) [54] for image synthesis. For each concept, we use Mixtral-8x7B to generate five different captions and we produce 35 images per caption. We set $\lambda_{dup} = 0.6$ for the duplicate removal [50] when using SSCD [52]. Similarly to T-MARS [43], we use FAST [12] as the text detection mechanism required for the text blurring of the OOD filtering. To mitigate data leakage, an additional SSCD-based filtering step eliminates images resembling any in the test sets of the traditional domain-specific datasets, using a lower similarity threshold of 0.45 to minimize false negatives. This process applied to our selected domains outputs two domain-specific datasets: PaS-B and PaS-F for *birds* and *food*, both of 1.2M images.

Dataset Evaluation: We assess the quality of the generated datasets from different perspectives: 1) variety and alignment with the corresponding domain, 2) transferability performance to different downstream tasks in the same domain (compared to other manually curated datasets), and 3) competitiveness with the SoA large-scale general-domain datasets generally used to pretrain backbones.

Domain-coverage evaluation: We compare the dataset itself with other existing manually curated datasets in the domain. We compare the concepts or categories present in each dataset with those of \mathcal{B} generated by Stage 1 of PaS. To do so, we compute the CLIP ViT-L/14 lexical embeddings [53] of all the concepts and class labels in the datasets of the domain (for iNat_{birds}, we take the common name of each bird species). We then compute the minimum cosine distance between each class label in every dataset of a given domain and any concept of \mathcal{B} . This will help us understand the proportion of supervised labels present in our automatically generated bank of concepts. Furthermore, for every domain, we compute the UMAP [44] of all the embeddings to qualitatively

assess the distribution of each dataset in the lexical space. Similarly, we also compute the visual embeddings of each image using a ResNet-152 pretrained on ImageNet-1K [17], and visualize them in a per-domain UMAP. Finally, we make use of the self-supervised dataset inspection tool *ProtoSim* [65] (with the default parameters), which allows us to find and compare the concept-level prototypes across datasets, enabling a comparative assessment of their richness.

Backbone pretraining: We focus most of our experimentation on Vision Transformers (ViTs) [19] due to their data-hungry behaviour [77]. Particularly, all the datasets will be evaluated using ViT-B/16. We use MoCo v3 [11] to pretrain the ViTs in a self-supervised way using the default parameters of the 300 epochs stated in the original paper [11]. In addition, we use NNCLR [22] with default parameters adapted to 500 epochs to train ResNet-18 and ResNet-50 [29] to study the applicability of PaS to CNN pretraining. During the evaluation, we test the transferability of the pretrained backbone on different downstream tasks, whose particular setups are described in the supplementary material.

4.2 Diversity and Domain-alignment of the Generated Datasets

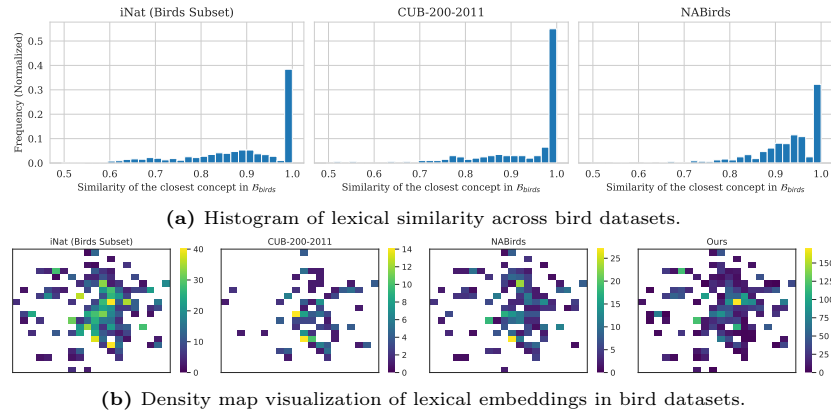


Fig. 3: Comparative analysis of lexical concept distributions in bird domain.

Distribution of lexical concepts: The first element of our pipeline is the LLM-generated concept bank \mathcal{B} , which should cover the target domain as much as possible. We compare the distributions of the lexical embeddings of the concepts in \mathcal{B} and the category labels of existing datasets. In *birds*, Figure 3 compares the lexical distribution of classes from three traditional datasets (CUB-200-2011, NABirds, iNat_{birds}) with concepts from PaS. Figure 3a shows the distribution of distances between each class and the nearest concept in \mathcal{B}_{birds} , indicating that most concepts from these datasets either closely match or are present in the LLM-generated concept bank, thus showing comprehensive coverage of the domain.

Additionally, Figure 3b reveals that \mathcal{B}_{birds} has a distribution more spread and varied across the embedding space compared to CUB-200-2011 and NABirds, and closely matching the granularity of iNat_{birds}. The high overlap between iNat_{birds} and \mathcal{B}_{birds} highlights that concepts generated by PaS align well with the target domain, indicating an effective dataset generation. Regarding the food domain, Figure 4 presents similar plots for Food-101, FoodX-251, and Food-2K. The histograms reveal a greater proximity of the concepts from Food-101 and FoodX-251 to \mathcal{B}_{food} compared to Food-2K, yet in all cases, most classes are very close to a PaS concept. Moreover, the density maps show that \mathcal{B}_{food} extensively covers the embedding space, effectively bridging the gaps between the classes of different datasets. The broad coverage and significant alignment with existing datasets in both the *bird* and *food* domains underscore the capacity of PaS-generated concepts to enrich dataset diversity and relevance to specific domains.

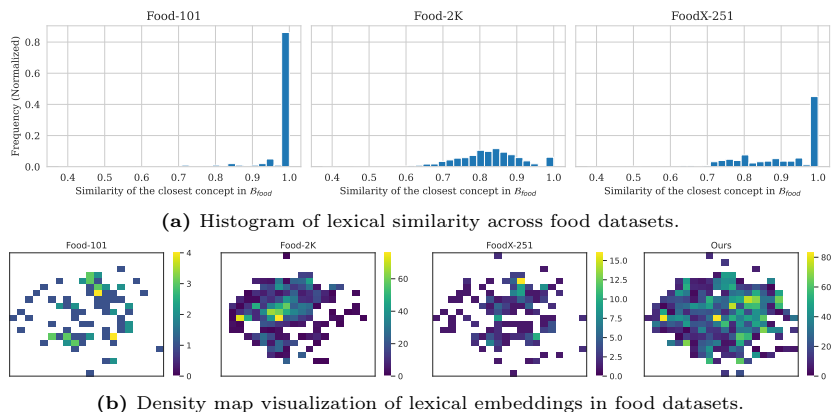


Fig. 4: Comparative analysis of lexical concept distributions in food domain.

Distribution of Image Embeddings: Figure 5 shows the density distribution of each dataset in the visual embedding space. In both the *birds* and *food* domains, we observe a notable alignment across all datasets. Specifically, *birds*, it is evident that larger datasets contribute to filling the embedding space more comprehensively. This effect is particularly pronounced in PaS-B, which achieves the most extensive coverage of the embedding space. Analyzing the density distribution, we find that while the CUB-200-2011 dataset exhibits densely populated regions, our dataset, alongside others, demonstrates a more uniform distribution across the embedding space. Similarly, in the *food* domain, Food-2K spans a broader area but includes numerous outliers, potentially indicating OOD images. PaS-F, in contrast, encompasses the embedding spaces of both Food-101 and Food-2K. Notably, it exhibits a uniform distribution of embeddings, balancing well between areas densely covered by other datasets and those

less populated, suggesting a comprehensive representation of the food domain. These observations underscore the effectiveness of PaS in automatically creating large-scale domain-specific datasets, in terms of image coverage and alignment with respect to existing datasets.

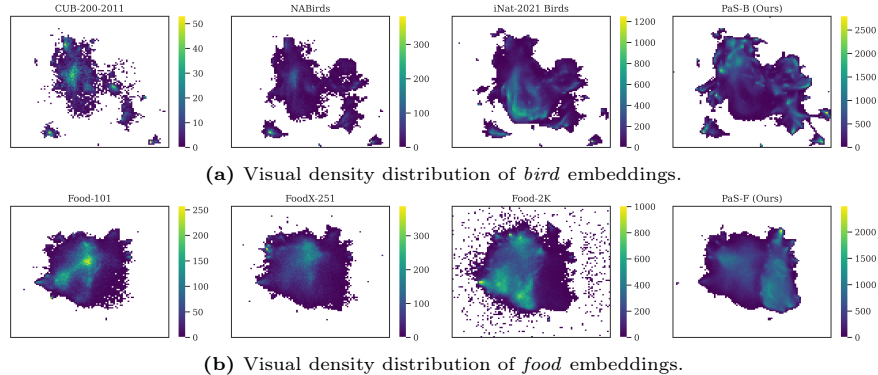


Fig. 5: Comparison of image embeddings distributions across Bird and Food domains.

Semantic richness analysis: Using *ProtoSim* [65], we conducted a comparison with the most comprehensive and diverse datasets in each domain, specifically $iNat_{birds}$ for *birds* and Food-2K for *food*. Within the *bird* domain, a total of 8159 prototypes were found to be shared, indicating a substantial overlap. Meanwhile, the $iNat_{birds}$ featured 10 unique prototypes in 25 images, in contrast to PaS-B, which boasted 23 unique prototypes in 358 images. In the *food* domain, 8144 prototypes were commonly identified. Food-2K exhibited 16 unique prototypes within 121 images, whereas PaS-F presented a total of 32, which were observed in 310 images. More details and visual examples of the prototypes can be found in the supplementary material. Results demonstrate the effectiveness of the PaS method in generating datasets that are not only comparable to established datasets in terms of semantic concepts but also includes unique concepts.

4.3 PaS Dataset evaluation

In-domain classification: We compare the pretraining capacity of PaS datasets against the current SoTA domain-specific datasets on Birds and Food domains. For this study, we pretrain ViT-B models using Food-2k and $iNat_{birds}$ subset (biggest datasets among their domain) and evaluate them in two popular evaluation datasets per domain. To show the capacity of PaS to adapt to different scales, we display the results for a total of four PaS datasets: PaS-B, PaS-F, PaS-B_{mini} and PaS-F_{mini}. While the first two maintain a scale similar to ImageNet-1k, the mini versions are enforced to have the same scale as their baseline counterparts. This ensures fairness when using a data-sensitive model

Table 1: Comparison on in-domain classification downstream tasks.

PT Data	CUB-200-2011		NABirds		PT Data	Food-101		FoodX-251	
	<i>k</i> -NN	Linear	<i>k</i> -NN	Linear		<i>k</i> -NN	Linear	<i>k</i> -NN	Linear
iNat _{birds}	19.68	30.57	11.16	21.16	Food-2K	65.36	78.73	50.63	60.99
PaS-B _{mini}	33.34	48.60	22.10	36.60	PaS-F _{mini}	66.75	79.68	53.68	64.29
PaS-B	46.36	68.92	42.31	56.36	PaS-F	77.31	86.84	61.86	71.61

such as ViT-B. We report Top-1 *k*-NN and Linear accuracies for all datasets. As can be seen in Table 1, PaS datasets prove to be better pretrainers even at the same scale. Mini datasets show the capacity of PaS to carefully collect, generate and select relevant images, improving by an average of more than 2.17% Food2k dataset, a dataset created and supervised by humans. For iNat_{birds} subset, we find the big improvements expected as it is a subset of a more general dataset instead of a fully focused one. When scaled to ImageNet-1k size, PaS datasets provide an overall average improvement of 21.66%.

PaS on ResNet backbones: Even if ViT architectures were our main focus, we analysed PaS on Resnets for the Food domain. In Table 2, we show how we still beat Food-2k on CNNs across different tasks such as image classification and object detection[†]. The increased amount of diversity and images provided by PaS benefit ResNet which are less data-hungry than transformers.

Table 2: Comparison on Food domain with ResNet backbones.

Backbone	PT Data	Food-101			FoodX-251			Oktoberfest [†]
		<i>k</i> -NN	Linear	FT	<i>k</i> -NN	Linear	FT	mAP
ResNet-18	Food-2k	56.93	77.15	82.14	45.90	60.18	63.98	60.70
	PaS-F	58.74	77.81	82.74	46.36	62.38	64.23	63.60
ResNet-50	Food-2k	61.58	81.16	87.03	48.17	64.76	70.24	61.10
	PaS-F	66.53	84.57	87.38	53.57	69.29	70.78	65.10

General and PaS datasets: Ultimately, we compare our PaS datasets with ImageNet-1k. As shown in Table 3, PaS datasets outperform ImageNet-1k as pretrainers on their respective domain by at least 12% across different datasets and classification tasks. This proves that, on the same scale, general datasets can not compete with domain-specific datasets in their domain. PaS enables the creation of domain-specific datasets that can compete in scale with general datasets while being as diverse as current domain-specific datasets, closing the gap between general and domain-specific datasets. In fact, we show how our food model trained on PaS_F manages to outperform by a great margin a supervised setup[†] trained in ImageNet-21k, a dataset almost twelve times bigger. This proves that,

for some domains, a modest amount of domain-specific images provides much more information than millions of general images.

Table 3: General and Domain-specific dataset comparison.

PT Data	# Images	Food101		FoodX-251		CUB		NABirds	
		k-NN	Linear	k-NN	Linear	k-NN	Linear	k-NN	Linear
ImageNet-21k [†]	14M	<u>59.31</u>	<u>80.64</u>	<u>40.10</u>	62.47	69.15	83.47	57.52	73.15
ImageNet-1k	1.2M	56.63	74.14	43.23	56.15	40.79	49.20	29.20	36.19
PaS-B _{Ours}	1.2M	-	-	-	-	<u>46.36</u>	<u>68.92</u>	<u>42.31</u>	<u>56.63</u>
PaS-F _{Ours}	1.2M	77.31	86.84	61.86	71.61	-	-	-	-

5 Limitations

Despite the high-quality datasets generated by PaS and its promising pretraining outcomes, it is crucial to recognize its limitations. The effectiveness of PaS is significantly dependent on the performance of external models, such as LLMs and Stable Diffusion. For instance, the initial step in the PaS pipeline requires the LLM to possess knowledge of the target domain. Additionally, variations in image quality across different domains by these models can introduce biases, possibly favoring some domains over others. This issue is more severe if the text-to-image models are not adequately trained for specific domains, like medical imaging. Nevertheless, the modular architecture of PaS provides a strategic advantage by facilitating the interchange of generative models to ones that are better suited for the intended domain, thereby offering adaptability and potentially mitigating this issue. While PaS reduces the cost of massive data collection for a given domain, it relies on large models with considerable computational requirements. Even if PaS can seamlessly collect large amounts of high-quality images, it might not be applicable in low-resources settings. Finally, we have not explored yet the usage of the text-image pairs that are generated by PaS. Despite the good results of training using only the visual output of PaS, the potential training of domain-specific vision-language models is still to be addressed.

6 Conclusions

In this paper, we introduced an innovative framework for autonomously generating domain-specific datasets on-demand. Its modular design facilitates the integration of various pretrained models, offering adaptability across different domains. Additionally, PaS incorporates an efficient pruning method to maintain high performance while reducing dataset size, tackling a major challenge in dataset curation. Our comprehensive analysis demonstrates PaS’s ability to

produce datasets that even exceed the richness and diversity of conventionally curated domain-specific SoTA datasets. When pretrained on PaS datasets, models display superior results compared to using traditional datasets of similar scale. More importantly, our framework enables the creation of larger datasets that lead to direct performance improvements on visual transformer models. Our empirical results show how our datasets outperform ImageNet-1k on all tested domains and even surpass ImageNet-21k supervised setup on the *food* domain while being twelve times smaller. This remarkable achievement not only validates the effectiveness of PaS but also illustrates that the paradigm shift it proposes can significantly enhance the effectiveness of model pretraining strategies by creating more efficient and specialized datasets.

References

1. Alayrac, J.B., Donahue, J., Luc, P., Miech, A., Barr, I., Hasson, Y., Lenc, K., Mensch, A., Millican, K., Reynolds, M., et al.: Flamingo: a visual language model for few-shot learning. *Advances in Neural Information Processing Systems* **35**, 23716–23736 (2022) [3](#)
2. Awais, M., Naseer, M., Khan, S., Anwer, R.M., Cholakkal, H., Shah, M., Yang, M.H., Khan, F.S.: Foundational models defining a new era in vision: A survey and outlook. *arXiv preprint arXiv:2307.13721* (2023) [3](#)
3. Azizi, S., Kornblith, S., Saharia, C., Norouzi, M., Fleet, D.J.: Synthetic data from diffusion models improves imagenet classification. *arXiv preprint arXiv:2304.08466* (2023) [3](#)
4. Bao, H., Dong, L., Wei, F.: Beit: Bert pre-training of image transformers. *arxiv* 2021. *arXiv preprint arXiv:2106.08254* [3](#)
5. Beaumont, R.: Clip retrieval: Easily compute clip embeddings and build a clip retrieval system with them. <https://github.com/rom1504/clip-retrieval> (2022) [34](#)
6. Bossard, L., Guillaumin, M., Van Gool, L.: Food-101—mining discriminative components with random forests. In: *Computer Vision—ECCV 2014: 13th European Conference, Zurich, Switzerland, September 6–12, 2014, Proceedings, Part VI* 13. pp. 446–461. Springer (2014) [2](#), [9](#), [26](#)
7. Cai, Z., Vasconcelos, N.: Cascade r-cnn: Delving into high quality object detection. In: *Proceedings of the IEEE conference on computer vision and pattern recognition*. pp. 6154–6162 (2018) [36](#)
8. Chang, H., Zhang, H., Barber, J., Maschinot, A., Lezama, J., Jiang, L., Yang, M.H., Murphy, K., Freeman, W.T., Rubinstein, M., et al.: Muse: Text-to-image generation via masked generative transformers. *arXiv preprint arXiv:2301.00704* (2023) [3](#)
9. Chen, K., Wang, J., Pang, J., Cao, Y., Xiong, Y., Li, X., Sun, S., Feng, W., Liu, Z., Xu, J., Zhang, Z., Cheng, D., Zhu, C., Cheng, T., Zhao, Q., Li, B., Lu, X., Zhu, R., Wu, Y., Dai, J., Wang, J., Shi, J., Ouyang, W., Loy, C.C., Lin, D.: MMDetection: Open mmlab detection toolbox and benchmark. *arXiv preprint arXiv:1906.07155* (2019) [36](#)
10. Chen, T., Kornblith, S., Norouzi, M., Hinton, G.: A simple framework for contrastive learning of visual representations. In: *International conference on machine learning*. pp. 1597–1607. PMLR (2020) [3](#)

11. Chen, X., Xie, S., He, K.: An empirical study of training self-supervised vision transformers. in 2021 IEEE International Conference on Computer Vision (ICCV). pp. 9620–9629 [10](#), [35](#)
12. Chen, Z., Wang, J., Wang, W., Chen, G., Xie, E., Luo, P., Lu, T.: Fast: Faster arbitrarily-shaped text detector with minimalist kernel representation (2021) [9](#)
13. Cherti, M., Beaumont, R., Wightman, R., Wortsman, M., Ilharco, G., Gordon, C., Schuhmann, C., Schmidt, L., Jitsev, J.: Reproducible scaling laws for contrastive language-image learning. In: Proceedings of the IEEE/CVF Conference on Computer Vision and Pattern Recognition. pp. 2818–2829 (2023) [3](#)
14. Contributors, M.: MMSegmentation: Openmmlab semantic segmentation toolbox and benchmark. <https://github.com/open-mmlab/mms Segmentation> (2020) [36](#)
15. Dehghani, M., Djolonga, J., Mustafa, B., Padlewski, P., Heek, J., Gilmer, J., Steiner, A.P., Caron, M., Geirhos, R., Alabdulmohsin, I., et al.: Scaling vision transformers to 22 billion parameters. In: International Conference on Machine Learning. pp. 7480–7512. PMLR (2023) [3](#)
16. Deng, J., Dong, W., Socher, R., Li, L.J., Li, K., Fei-Fei, L.: Imagenet: A large-scale hierarchical image database. In: 2009 IEEE conference on computer vision and pattern recognition. pp. 248–255. Ieee (2009) [3](#), [26](#)
17. Deng, J., Dong, W., Socher, R., Li, L.J., Li, K., Fei-Fei, L.: Imagenet: A large-scale hierarchical image database. In: 2009 IEEE Conference on Computer Vision and Pattern Recognition. pp. 248–255 (2009). <https://doi.org/10.1109/CVPR.2009.5206848> [10](#)
18. Dosovitskiy, A., Beyer, L., Kolesnikov, A., Weissenborn, D., Zhai, X., Unterthiner, T., Dehghani, M., Minderer, M., Heigold, G., Gelly, S., Uszkoreit, J., Houlsby, N.: An image is worth 16x16 words: Transformers for image recognition at scale. In: 9th International Conference on Learning Representations, ICLR 2021, Virtual Event, Austria, May 3-7, 2021. OpenReview.net (2021), <https://openreview.net/forum?id=YicbFdNTTy> [2](#)
19. Dosovitskiy, A., Beyer, L., Kolesnikov, A., Weissenborn, D., Zhai, X., Unterthiner, T., Dehghani, M., Minderer, M., Heigold, G., Gelly, S., Uszkoreit, J., Houlsby, N.: An image is worth 16x16 words: Transformers for image recognition at scale. ICLR (2021) [10](#)
20. Douze, M., Guzhva, A., Deng, C., Johnson, J., Szilvasy, G., Mazaré, P.E., Lomeli, M., Hosseini, L., Jégou, H.: The faiss library (2024) [34](#)
21. Doveh, S., Arbelle, A., Harary, S., Schwartz, E., Herzig, R., Giryes, R., Feris, R., Panda, R., Ullman, S., Karlinsky, L.: Teaching structured vision & language concepts to vision & language models. In: Proceedings of the IEEE/CVF Conference on Computer Vision and Pattern Recognition. pp. 2657–2668 (2023) [3](#), [7](#), [34](#)
22. Dwivedi, D., Aytar, Y., Tompson, J., Sermanet, P., Zisserman, A.: With a little help from my friends: Nearest-neighbor contrastive learning of visual representations. In: Proceedings of the IEEE/CVF International Conference on Computer Vision. pp. 9588–9597 (2021) [3](#), [10](#), [35](#)
23. Fang, Y., Wang, W., Xie, B., Sun, Q., Wu, L., Wang, X., Huang, T., Wang, X., Cao, Y.: Eva: Exploring the limits of masked visual representation learning at scale. In: Proceedings of the IEEE/CVF Conference on Computer Vision and Pattern Recognition. pp. 19358–19369 (2023) [3](#)
24. Girdhar, R., El-Nouby, A., Liu, Z., Singh, M., Alwala, K.V., Joulin, A., Misra, I.: Imagebind: One embedding space to bind them all. In: Proceedings of the IEEE/CVF Conference on Computer Vision and Pattern Recognition. pp. 15180–15190 (2023) [3](#)

25. Grill, J.B., Strub, F., Altché, F., Tallec, C., Richemond, P., Buchatskaya, E., Doersch, C., Avila Pires, B., Guo, Z., Gheshlaghi Azar, M., et al.: Bootstrap your own latent—a new approach to self-supervised learning. *Advances in neural information processing systems* **33**, 21271–21284 (2020) [3](#)
26. Hammoud, H.A.A.K., Itani, H., Pizzati, F., Torr, P., Bibi, A., Ghanem, B.: Synthclip: Are we ready for a fully synthetic clip training? *arXiv preprint arXiv:2402.01832* (2024) [2](#), [3](#)
27. He, K., Chen, X., Xie, S., Li, Y., Dollár, P., Girshick, R.: Masked autoencoders are scalable vision learners. In: *Proceedings of the IEEE/CVF conference on computer vision and pattern recognition*. pp. 16000–16009 (2022) [3](#)
28. He, K., Fan, H., Wu, Y., Xie, S., Girshick, R.: Momentum contrast for unsupervised visual representation learning. In: *Proceedings of the IEEE/CVF conference on computer vision and pattern recognition*. pp. 9729–9738 (2020) [3](#)
29. He, K., Zhang, X., Ren, S., Sun, J.: Deep residual learning for image recognition. In: *Proceedings of the IEEE conference on computer vision and pattern recognition*. pp. 770–778 (2016) [10](#)
30. Huang, R., Long, Y., Han, J., Xu, H., Liang, X., Xu, C., Liang, X.: Nlip: Noise-robust language-image pre-training. In: *Proceedings of the AAAI Conference on Artificial Intelligence*. vol. 37, pp. 926–934 (2023) [3](#)
31. Jia, C., Yang, Y., Xia, Y., Chen, Y.T., Parekh, Z., Pham, H., Le, Q., Sung, Y.H., Li, Z., Duerig, T.: Scaling up visual and vision-language representation learning with noisy text supervision. In: *International conference on machine learning*. pp. 4904–4916. PMLR (2021) [3](#)
32. Jiang, A.Q., Sablayrolles, A., Roux, A., Mensch, A., Savary, B., Bamford, C., Chaplot, D.S., Casas, D.d.l., Hanna, E.B., Bressand, F., et al.: Mixtral of experts. *arXiv preprint arXiv:2401.04088* (2024) [9](#), [34](#)
33. Kaur, P., Sikka, K., Wang, W., Belongie, S., Divakaran, A.: Foodx-251: a dataset for fine-grained food classification. *arXiv preprint arXiv:1907.06167* (2019) [9](#), [26](#)
34. Kim, D., Angelova, A., Kuo, W.: Contrastive feature masking open-vocabulary vision transformer. In: *Proceedings of the IEEE/CVF International Conference on Computer Vision*. pp. 15602–15612 (2023) [3](#)
35. Kirillov, A., Mintun, E., Ravi, N., Mao, H., Rolland, C., Gustafson, L., Xiao, T., Whitehead, S., Berg, A.C., Lo, W.Y., et al.: Segment anything. *arXiv preprint arXiv:2304.02643* (2023) [3](#)
36. Kolesnikov, A., Beyer, L., Zhai, X., Puigcerver, J., Yung, J., Gelly, S., Houlsby, N.: Big transfer (bit): General visual representation learning. In: *Computer Vision—ECCV 2020: 16th European Conference, Glasgow, UK, August 23–28, 2020, Proceedings, Part V* 16. pp. 491–507. Springer (2020) [3](#)
37. Li, A.C., Brown, E.L., Efros, A.A., Pathak, D.: Internet explorer: Targeted representation learning on the open web. In: *International Conference on Machine Learning*. pp. 19385–19406. PMLR (2023) [3](#)
38. Li, G., Duan, N., Fang, Y., Gong, M., Jiang, D.: Unicoder-vl: A universal encoder for vision and language by cross-modal pre-training. In: *Proceedings of the AAAI conference on artificial intelligence*. vol. 34, pp. 11336–11344 (2020) [3](#)
39. Li, J., Li, D., Savarese, S., Hoi, S.: Blip-2: Bootstrapping language-image pre-training with frozen image encoders and large language models. *arXiv preprint arXiv:2301.12597* (2023) [3](#)
40. Lin, T.Y., Maire, M., Belongie, S., Hays, J., Perona, P., Ramanan, D., Dollár, P., Zitnick, C.L.: Microsoft coco: Common objects in context. In: *Computer Vision—ECCV 2014: 13th European Conference, Zurich, Switzerland, September 6–12, 2014, Proceedings, Part V* 13. pp. 740–755. Springer (2014) [36](#)

41. Liu, Z., Lin, Y., Cao, Y., Hu, H., Wei, Y., Zhang, Z., Lin, S., Guo, B.: Swin transformer: Hierarchical vision transformer using shifted windows. In: Proceedings of the IEEE/CVF international conference on computer vision. pp. 10012–10022 (2021) [23](#), [24](#)
42. Mahajan, D., Girshick, R., Ramanathan, V., He, K., Paluri, M., Li, Y., Bharambe, A., Van Der Maaten, L.: Exploring the limits of weakly supervised pretraining. In: Proceedings of the European conference on computer vision (ECCV). pp. 181–196 (2018) [3](#)
43. Maini, P., Goyal, S., Lipton, Z.C., Kolter, J.Z., Raghunathan, A.: T-mars: Improving visual representations by circumventing text feature learning. In: The Twelfth International Conference on Learning Representations (2023) [8](#), [9](#), [34](#)
44. McInnes, L., Healy, J., Melville, J.: Umap: Uniform manifold approximation and projection for dimension reduction. arXiv preprint arXiv:1802.03426 (2018) [9](#)
45. Min, W., Liu, L., Wang, Z., Luo, Z., Wei, X., Wei, X., Jiang, S.: Isia food-500: A dataset for large-scale food recognition via stacked global-local attention network. In: Proceedings of the 28th ACM International Conference on Multimedia. pp. 393–401 (2020) [2](#)
46. Min, W., Wang, Z., Liu, Y., Luo, M., Kang, L., Wei, X., Wei, X., Jiang, S.: Large scale visual food recognition. IEEE Transactions on Pattern Analysis and Machine Intelligence (2023) [2](#), [9](#), [25](#), [26](#), [30](#)
47. Minderer, M., Gritsenko, A., Stone, A., Neumann, M., Weissenborn, D., Dosovitskiy, A., Mahendran, A., Arnab, A., Dehghani, M., Shen, Z., et al.: Simple open-vocabulary object detection. In: European Conference on Computer Vision. pp. 728–755. Springer (2022) [3](#)
48. Mündler, N., He, J., Jenko, S., Vechev, M.: Self-contradictory hallucinations of large language models: Evaluation, detection and mitigation. In: The Twelfth International Conference on Learning Representations (2024), <https://openreview.net/forum?id=EmQS0i1X2f> [6](#)
49. Ngatchou, P., Zarei, A., El-Sharkawi, A.: Pareto multi objective optimization. In: Proceedings of the 13th International Conference on, Intelligent Systems Application to Power Systems. pp. 84–91 (2005). <https://doi.org/10.1109/ISAP.2005.1599245> [8](#)
50. Oquab, M., Darcet, T., Moutakanni, T., Vo, H., Szafraniec, M., Khalidov, V., Fernandez, P., Haziza, D., Massa, F., El-Nouby, A., et al.: Dinov2: Learning robust visual features without supervision. arXiv preprint arXiv:2304.07193 (2023) [1](#), [2](#), [3](#), [9](#)
51. Pham, H., Dai, Z., Ghiasi, G., Kawaguchi, K., Liu, H., Yu, A.W., Yu, J., Chen, Y.T., Luong, M.T., Wu, Y., et al.: Combined scaling for zero-shot transfer learning. Neurocomputing **555**, 126658 (2023) [3](#)
52. Pizzi, E., Roy, S.D., Ravindra, S.N., Goyal, P., Douze, M.: A self-supervised descriptor for image copy detection. In: Proceedings of the IEEE/CVF Conference on Computer Vision and Pattern Recognition. pp. 14532–14542 (2022) [7](#), [9](#), [34](#)
53. Radford, A., Kim, J.W., Hallacy, C., Ramesh, A., Goh, G., Agarwal, S., Sastry, G., Askell, A., Mishkin, P., Clark, J., et al.: Learning transferable visual models from natural language supervision. In: International conference on machine learning. pp. 8748–8763. PMLR (2021) [3](#), [7](#), [9](#)
54. Rombach, R., Blattmann, A., Lorenz, D., Esser, P., Ommer, B.: High-resolution image synthesis with latent diffusion models. In: Proceedings of the IEEE/CVF Conference on Computer Vision and Pattern Recognition (CVPR). pp. 10684–10695 (June 2022) [2](#), [3](#), [7](#), [9](#), [34](#)

55. Russakovsky, O., Deng, J., Su, H., Krause, J., Satheesh, S., Ma, S., Huang, Z., Karpathy, A., Khosla, A., Bernstein, M., et al.: Imagenet large scale visual recognition challenge. *International journal of computer vision* **115**, 211–252 (2015) [2](#), [3](#), [26](#), [35](#)
56. Satopaa, V., Albrecht, J., Irwin, D., Raghavan, B.: Finding a "knee" in a haystack: Detecting knee points in system behavior. In: 2011 31st international conference on distributed computing systems workshops. pp. 166–171. IEEE (2011) [8](#)
57. Schuhmann, C., Beaumont, R., Vencu, R., Gordon, C., Wightman, R., Cherti, M., Coombes, T., Katta, A., Mullis, C., Wortsman, M., et al.: Laion-5b: An open large-scale dataset for training next generation image-text models. *Advances in Neural Information Processing Systems* **35**, 25278–25294 (2022) [2](#), [3](#), [9](#)
58. Shao, W., Zhao, X., Ge, Y., Zhang, Z., Yang, L., Wang, X., Shan, Y., Luo, P.: Not all models are equal: predicting model transferability in a self-challenging fisher space. In: *European Conference on Computer Vision*. pp. 286–302. Springer (2022) [24](#)
59. Shin, G., Xie, W., Albanie, S.: Namedmask: Distilling segmenters from complementary foundation models. In: *Proceedings of the IEEE/CVF Conference on Computer Vision and Pattern Recognition*. pp. 4960–4969 (2023) [3](#)
60. Steiner, A., Kolesnikov, A., Zhai, X., Wightman, R., Uszkoreit, J., Beyer, L.: How to train your vit? data, augmentation, and regularization in vision transformers. *arXiv preprint arXiv:2106.10270* (2021) [35](#)
61. Tian, Y., Fan, L., Chen, K., Katabi, D., Krishnan, D., Isola, P.: Learning vision from models rivals learning vision from data. *arXiv preprint arXiv:2312.17742* (2023) [2](#), [3](#)
62. Touvron, H., Martin, L., Stone, K., Albert, P., Almahairi, A., Babaei, Y., Baid, A., Baevski, N., Batra, S., Bhargava, P., Bhosale, S., et al.: Llama 2: Open foundation and fine-tuned chat models. *arXiv preprint arXiv:2307.09288* (2023) [9](#), [34](#)
63. Van Horn, G., Branson, S., Farrell, R., Haber, S., Barry, J., Ipeirotis, P., Perona, P., Belongie, S.: Building a bird recognition app and large scale dataset with citizen scientists: The fine print in fine-grained dataset collection. In: *Proceedings of the IEEE Conference on Computer Vision and Pattern Recognition (CVPR)* (June 2015) [2](#), [9](#), [26](#)
64. Van Horn, G., Cole, E., Beery, S., Wilber, K., Belongie, S., Mac Aodha, O.: Benchmarking representation learning for natural world image collections. In: *Proceedings of the IEEE/CVF conference on computer vision and pattern recognition*. pp. 12884–12893 (2021) [9](#), [25](#), [26](#)
65. van Noord, N.: Prototype-based dataset comparison. In: *ICCV* (2023) [10](#), [12](#), [30](#)
66. Wah, C., Branson, S., Welinder, P., Perona, P., Belongie, S.: The caltech-ucsd birds-200-2011 dataset (2011) [2](#), [9](#), [26](#)
67. Wang, Z., Luo, Y., Zheng, L., Huang, Z., Baktashmotlagh, M.: How far pre-trained models are from neural collapse on the target dataset informs their transferability. In: *Proceedings of the IEEE/CVF International Conference on Computer Vision*. pp. 5549–5558 (2023) [24](#)
68. Wang, Z., Yu, J., Yu, A.W., Dai, Z., Tsvetkov, Y., Cao, Y.: Simvlm: Simple visual language model pretraining with weak supervision. *arXiv preprint arXiv:2108.10904* (2021) [3](#)
69. Woo, S., Debnath, S., Hu, R., Chen, X., Liu, Z., Kweon, I.S., Xie, S.: Convnext v2: Co-designing and scaling convnets with masked autoencoders. In: *Proceedings of the IEEE/CVF Conference on Computer Vision and Pattern Recognition*. pp. 16133–16142 (2023) [3](#)

70. Wu, X., Fu, X., Liu, Y., Lim, E.P., Hoi, S.C., Sun, Q.: A large-scale benchmark for food image segmentation. In: Proceedings of the 29th ACM International Conference on Multimedia. pp. 506–515 (2021) [23](#), [24](#), [36](#)
71. Xiao, B., Wu, H., Xu, W., Dai, X., Hu, H., Lu, Y., Zeng, M., Liu, C., Yuan, L.: Florence-2: Advancing a unified representation for a variety of vision tasks (2023), <https://api.semanticscholar.org/CorpusID:265128818> [3](#)
72. Xiao, T., Liu, Y., Zhou, B., Jiang, Y., Sun, J.: Unified perceptual parsing for scene understanding. In: Proceedings of the European Conference on Computer Vision (ECCV). pp. 418–434 (2018) [24](#), [36](#)
73. Xie, Z., Zhang, Z., Cao, Y., Lin, Y., Bao, J., Yao, Z., Dai, Q., Hu, H.: Simmim: A simple framework for masked image modeling. In: Proceedings of the IEEE/CVF Conference on Computer Vision and Pattern Recognition. pp. 9653–9663 (2022) [3](#)
74. Xu, H., Xie, S., Tan, X.E., Huang, P.Y., Howes, R., Sharma, V., Li, S.W., Ghosh, G., Zettlemoyer, L., Feichtenhofer, C.: Demystifying clip data. arXiv preprint arXiv:2309.16671 (2023) [4](#)
75. You, K., Liu, Y., Wang, J., Long, M.: Logme: Practical assessment of pre-trained models for transfer learning. In: International Conference on Machine Learning. pp. 12133–12143. PMLR (2021) [24](#)
76. Yu, J., Wang, Z., Vasudevan, V., Yeung, L., Seyedhosseini, M., Wu, Y.: Coca: Contrastive captioners are image-text foundation models. arXiv preprint arXiv:2205.01917 (2022) [3](#)
77. Zhai, X., Kolesnikov, A., Houlsby, N., Beyer, L.: Scaling vision transformers. In: Proceedings of the IEEE/CVF Conference on Computer Vision and Pattern Recognition. pp. 12104–12113 (2022) [3](#), [10](#)
78. Zheng, S., Lu, J., Zhao, H., Zhu, X., Luo, Z., Wang, Y., Fu, Y., Feng, J., Xiang, T., Torr, P.H., Zhang, L.: Rethinking semantic segmentation from a sequence-to-sequence perspective with transformers. In: CVPR (2021) [24](#)
79. Zheng, Y., Yang, H., Zhang, T., Bao, J., Chen, D., Huang, Y., Yuan, L., Chen, D., Zeng, M., Wen, F.: General facial representation learning in a visual-linguistic manner. In: Proceedings of the IEEE/CVF Conference on Computer Vision and Pattern Recognition. pp. 18697–18709 (2022) [3](#)
80. Zhou, K., Yang, J., Loy, C.C., Liu, Z.: Conditional prompt learning for vision-language models. In: Proceedings of the IEEE/CVF Conference on Computer Vision and Pattern Recognition. pp. 16816–16825 (2022) [3](#)
81. Ziller, A., Hansjakob, J., Rusinov, V., Zügner, D., Vogel, P., Günnemann, S.: Oktoberfest food dataset. arXiv preprint arXiv:1912.05007 (2019) [36](#)

A Additional Evaluations

To further validate the capacity of our PaS datasets, we evaluate them on three additional downstream tasks: Finetuned linear classification, Semantic Segmentation and Model Transferability.

A.1 Finetuning Downstream Task

In Table 4, we show the results obtained when applying the finetuning downstream task to the backbones (ViT-B/16) pretrained using the PaS datasets, curated domain-specific datasets and large-scale general datasets (ImageNet). More details on the finetuning settings are described in Appendix D.3.

Table 4: Results of finetuning the pretrained backbones to two datasets per domain. In all the cases, the architecture used is ViT-B/16. † denotes backbones pretrained in a supervised way.

Pretraining Data	Food-101	FoodX-251	Pretraining Data	CUB-200	NABirds
ImageNet-21K†	86.29	70.08	ImageNet-21K†	76.00	64.80
ImageNet-1K	87.05	71.66	ImageNet-1K	78.46	<u>73.17</u>
Food-2K	87.92	72.47	iNat _{birds}	76.75	69.92
PaS-F	89.13	74.34	PaS-B	82.90	77.11
PaS-F _{mini}	<u>88.27</u>	<u>73.61</u>	PaS-B _{mini}	<u>79.50</u>	73.00

To further illuminate the efficacy of our PaS datasets in enhancing model performance, Figure 6 and Figure 7 provide a comprehensive visual comparison across various pretraining data sources. These figures underscore not only the superior accuracy our models achieve when pretrained on the PaS datasets but also highlight the efficiency of our approach. Despite the comparatively smaller size of our datasets relative to the expansive ImageNet-1K and ImageNet-21K, the results showcased here confirm that our models surpass the performance metrics of those pretrained on the larger datasets. This visualization serves to underscore the remarkable balance we have achieved between computational cost and accuracy, demonstrating that our PaS datasets enable the attainment of high model accuracy with significantly fewer forward passes during pretraining.

In the context of this downstream task, focusing first on *food*, the PaS datasets exhibit better performance when compared to existing manually curated datasets, whether they are general or domain-specific, of a similar size. A similar pattern is observed for *birds*, reinforcing the effectiveness of PaS datasets in these scenarios. Specifically, the complete PaS datasets (PaS-F and PaS-B) stand out as the most effective pretraining datasets across the four target tasks we examined, showing improvements ranging from 0.73% to 3.94% over the second-best dataset.



Fig. 6: Comparison of the accuracy achieved by ViT-B/16 on *food* when pretrained on different datasets. The X axis (log scale) represents the size of the pretraining set, and the Y axis the accuracy. Models using PaS data are highlighted with a black border. The shape of the marker indicates the downstream task. The size of the bubble represents the number of forward passes used for each pretraining (the bigger, the more computationally intensive the pretraining is).

Furthermore, the smaller version of the PaS datasets, known as *mini* (which is half the size of PaS-F and PaS-B), performs as the second best in three out of four tasks. The sole deviation is seen in NABirds, where it ranks third, only 0.17% below the second rank (ImageNet-1K, which is approximately two to three times larger).

These results go in line with the observations highlighted in the main paper: domain-specific datasets are better pretrainers than general-domain datasets (both in supervised and self-supervised settings), even with a much smaller size. Besides, domain-focused datasets generated by PaS outperform existing state-of-the-art manually curated domain-specific image collections for this purpose.



Fig. 7: Comparison of the final accuracy achieved by ViT-B/16 on *birds* when pretrained on different datasets. The X axis (log scale) represents the size of the pretraining set, and the Y axis the accuracy. Models using PaS data are highlighted with a black border. The shape of the marker indicates the downstream task. The size of the bubble represents the number of forward passes used for each pretraining (the bigger, the more computationally intensive the pretraining is).

A.2 Semantic Segmentation

In addition to the classification and object detection tasks already considered, we evaluate the suitability of different datasets as pretrainers for semantic segmentation. Particularly, we consider the FoodSeg103 [70] dataset for our evaluations.

Table 5 contains the results obtained for this downstream task (more details on the setup can be found in Appendix D.3). At first, we show the results provided by the FoodSeg103 paper [70], and the last two rows contain the results obtained by us when using the weights pretrained on Food-2K and PaS-F. It is important to note that we use the same configuration as the other experiments.

ViT-B pretrained with the PaS dataset outperforms the rest of the backbones (both ViT-B and Swin [41]) trained on different datasets. Significant enhancements are observed in both mean Intersection over Union (mIoU) and mean accuracy (mAcc). These findings suggest that specialized datasets like PaS can

benefit not only classification and object detection, but also dense tasks like semantic segmentation.

Table 5: Results on the downstream task of semantic segmentation for the dataset FoodSeg103 [70]. Results for ImageNet-21K pretraining have been taken from the FoodSeg103 paper [70].

Pretrain Data	Method	Backbone	mIoU	mAcc
ImageNet-21K	SETR [78]	ViT-B/16	41.3	52.7
	UperNet [72]	Swin-S [41]	41.6	53.6
		Swin-B [41]	41.2	53.9
Food-2K	UperNet [72]	ViT-B/16	38.1	51.1
PaS-F		ViT-B/16	42.5	55.5

A.3 Transferability Metrics

Recent works [58,67,75] use a variety of metrics to evaluate the transfer learning capacity of backbones. Metrics such as LogME [75] and NCTI [67] show a high correlation with the transfer learning capacity of the models, helping us evaluate the transferability capacity of a model without fine-tuning or linear probing it. As a further evaluation, we compare the transferability of the models trained on PaS and PaS-Mini datasets with the ones trained on Food-2K and ImageNet over various target datasets.

We report LogME [75] and NCTI [67] on three food datasets. As can be seen in Fig. 8, models trained on the PaS dataset provide much higher transferability in both metrics, except in the case of Food-2K. As expected, models trained on Food-2K still provide better transferability when evaluated on the same dataset. While having the same size, PaS-Mini still beats Food-2K on Food-101 and FoodX-251 datasets, showing a higher transferability capacity. Furthermore, depending on the metrics, PaS-Mini is able to beat ImageNet21k, which has 23 times more images.

B Dataset Statistics

In this section, we compare the sizes of our datasets and current SoTA datasets. Next, we explain how PaS datasets evolve step by step.

B.1 Dataset Sizes

Appendix B.1 displays the sizes of the different existing generic and domain-specific datasets, as well as the PaS datasets created and tested in our research.

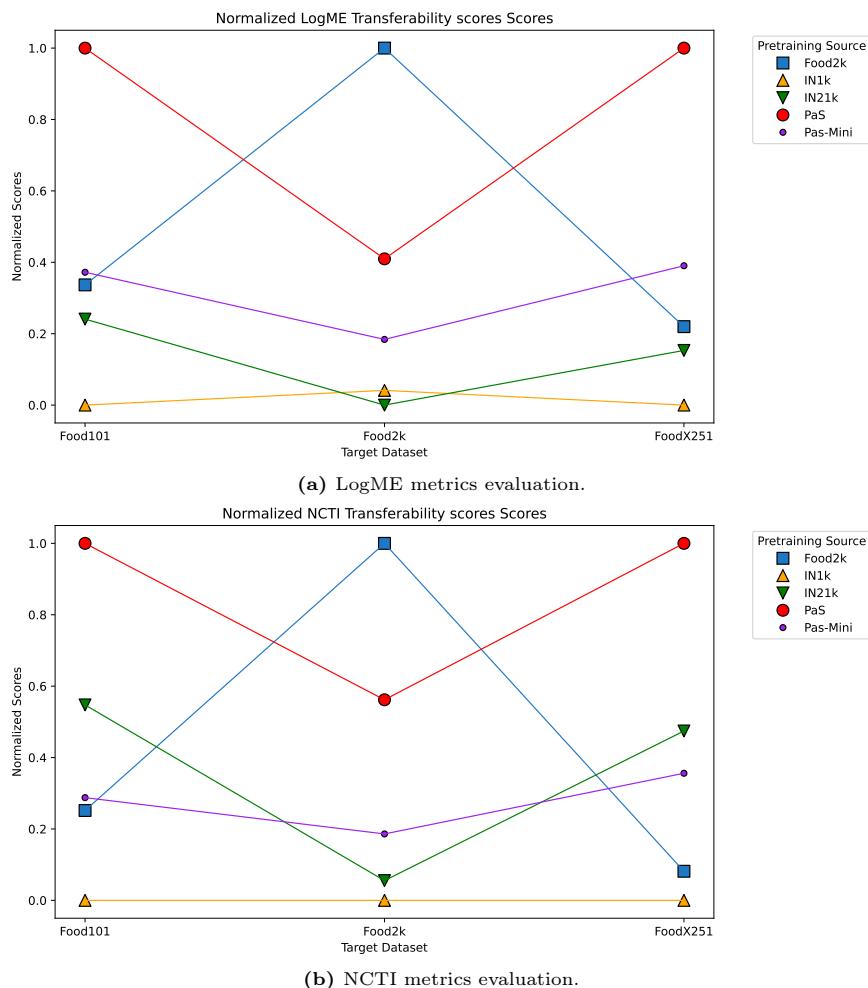


Fig. 8: Transferability evaluation. We evaluate the transferability of the models pretrained on different datasets. Values of each ranking (same target dataset and metrics) have been normalized for visualization purposes.

In the two studied domains (*food* and *birds*), we have compared with the largest existing supervised counterpart: Food-2K [46] and $iNat_{birds}$ (the subset of bird species of the $iNat$ -2021 dataset [64]). We can see that both datasets are considerably bigger than the others in the domain, and they also present a greater variety and domain coverage (larger category set). Thus, they are the best option as manually curated baselines.

Regarding the PaS datasets, as explained in the main paper, the versatility of the PaS pruning pipeline allows us to tailor a target final size. In this way, we have generated two versions per domain to enable fair comparisons: one with a

Table 6: Number of categories and images of the considered datasets. Only images used for training are counted (i.e. training set). * denotes the number of concepts created by the PaS pipeline rather than traditional categories.

Dataset	Domain	Number of classes	Number of images
ImageNet-1K [16]	General	1,000	1,281,167
ImageNet-21K [55]	General	21,841	14,197,122
Food-101 [6]	Food	101	75,750
FoodX-251 [33]	Food	251	118,475
Food-2K [46]	Food	2,000	620,191
CUB-200-2011 [66]	Birds	200	5,994
NABirds [63]	Birds	555	23,929
iNat _{birds} [64]	Birds	1,486	414,847
PaS-F _{mini}	Food	5,014*	627,703
PaS-F	Food	5,014*	1,177,810
PaS-B _{mini}	Birds	3,337*	449,999
PaS-B	Birds	3,337*	1,200,241

similar size to ImageNet-1K, and a *mini* variant comparable to the supervised equivalent.

B.2 Impact of the PaS Stages in the Datasets

In this subsection, we detail the evolution of the dataset generated by PaS through the different steps of the pipeline.

Food Domain. The size of the initial set of concepts, \mathcal{B}_0 , was 248. After the concept expansion and validation, we ended up with a concept bank \mathcal{B} of 5014 elements. In Table 7, we can observe the size of the real and synthetic elements of the dataset after different filtering steps.

Table 7: Evolution of the size of PaS-F and PaS-F_{mini} at different stages of the PaS pipeline.

	Raw	Deduplication	Pareto-OOD (PaS-F)	Pareto-OOD (PaS-F _{mini})
Real	723,888	652,262	465,173	88,084
Synthetic	877,450	877,450	712,637	539,619
Total	1,601,338	1,529,712	1,177,810	627,703

Regarding the deduplication stage, only real images were removed (since no duplicates were found among the synthetic images). Figure 9 contains three groups of images detected as duplicated by the pipeline. As we can see, some

of them are exact duplicates, others are different crops of the same image, and the last one simply contains two very similar scenes. The fact that no synthetic images have been removed in this step highlights the variety achieved by the image generation process.



Fig. 9: Examples of duplicates found and removed in the creation of PaS-F.

Regarding the Pareto optimization-based removal, we show in Table 7 the figures for both PaS-F and PaS-F_{mini}. While the removal for the former is balanced between synthetic and real images, as we keep removing progressive Pareto-fronts, the method seems to favour synthetic images. In order to understand this behaviour, we show in Figure 10 examples of images removed at different steps of the Pareto optimization-based filtering: the lower the row, the less OOD PaS consider those images. The first thing, we can highlight, is that there is a clear correlation between the Pareto position and the suitability or the degree of relation of the images with the *food* domain (which supports the quality PaS). The synthetic image generation is guided to be within the domain, so most of the images should be well aligned with the domain. If some images are not, this should be due to a problem with the caption (for example, the houses that appear in the first Pareto front). Once we get rid of those kinds of images, the rest are good within the domain, leading to a greater proportion of real images getting removed. Moreover, as we go on with the Pareto-pruning, it is more likely to remove images that are actually relevant (like in the 100th Pareto front).

Finally, Figure 11 contains 60 random examples (30 real and 30 synthetic) from PaS-F. The examples show great quality and alignment with the *food* domain, proving the suitability of PaS for the autonomous creation of domain-specific datasets.

Birds Domain. Similarly, we display in Table 8 the number of real and synthetic *bird* images at different stages of the PaS pipeline.

Figure 12 displays various sets of duplicate images discovered in the first filtering step. In contrast to the case of *food*, in this domain, some synthetic images are flagged as duplicates. This is the case in the last row, where the same caption leads to very similar images. Another example is the flock of birds: while different, they are visually too similar to SSCD, leading to duplicate detection.

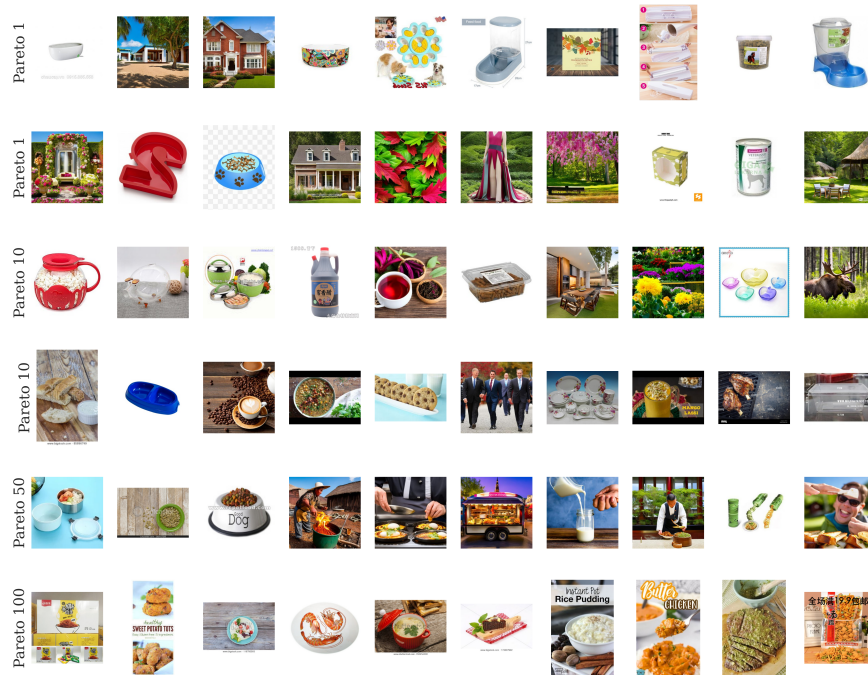


Fig. 10: Examples of images removed during the Pareto-based removal for the *food* domain. “Pareto n ” refers to images belonging to the n -th Pareto front (removed in the n -th iteration).

Table 8: Evolution of the size of PaS-B and PaS-B_{mini} at different stages of the PaS pipeline.

	Raw	Deduplication	Pareto-OOD (PaS-B)	Pareto-OOD (PaS-B mini)
Real	873,464	799,739	643,989	64,215
Synthetic	583,975	578,626	556,252	385,784
Total	1,457,439	1,378,365	1,200,241	449,999

However, real images still represent the vast majority of images removed in this step due to the presence of identical or almost identical images on the Web. Indeed, some of them are just variations of the same images (such as examples in the second row).

In the Pareto-based image curation step, we observe the same pattern as in the case of *food*: the further we advance, the more penalized the real images with respect to the synthetic ones. As illustrated in the instances presented in Figure 13, it is evident that the initial images eliminated are not closely related to the specific domain of interest, namely, *birds*. Subsequent iterations (bottom rows) exhibit images that are more pertinent to the target domain. This

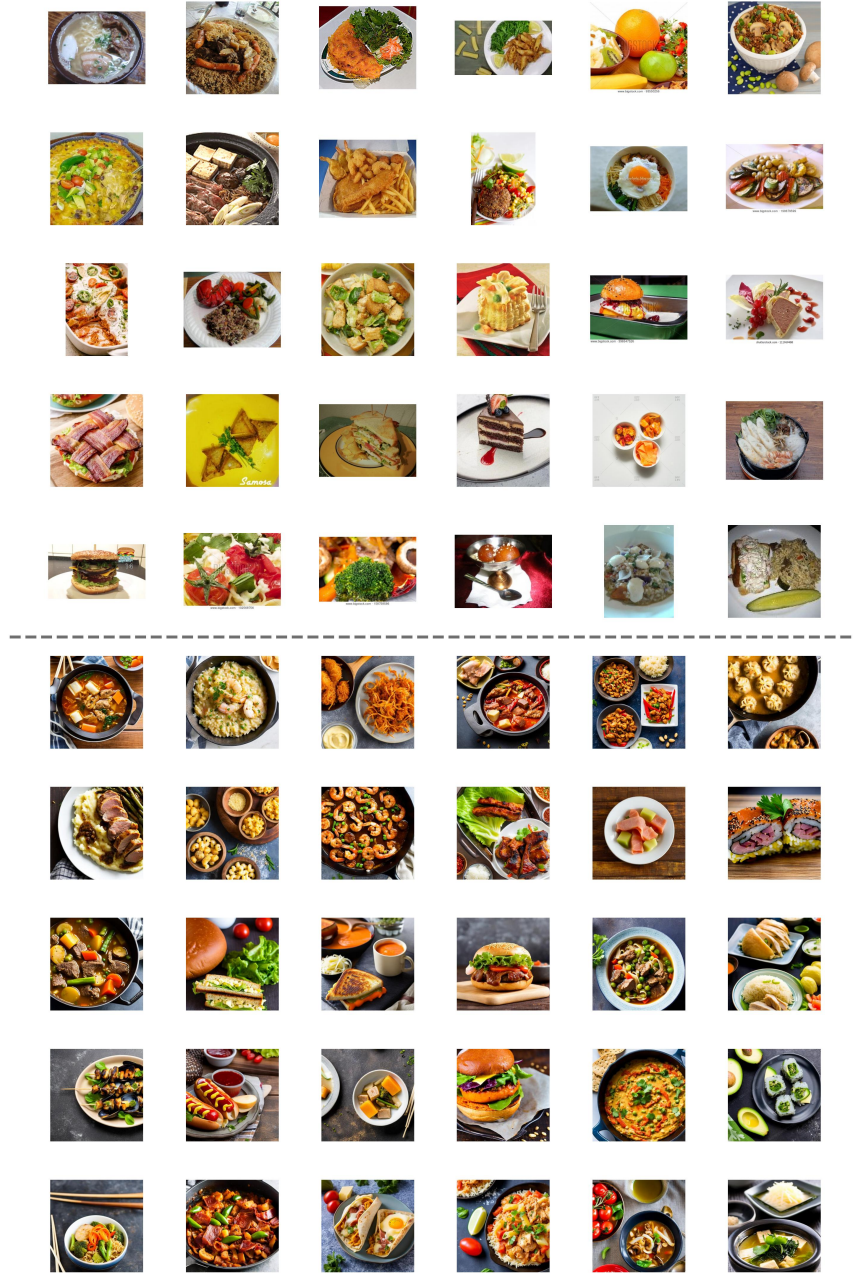


Fig. 11: Examples from PaS-F dataset. The first 5 rows correspond to real images (from LAION-5B). The 5 bottom rows are generated by SD 2.1.



Fig. 12: Examples of duplicates found and removed in the creation of PaS-B. The first two rows are sets of duplicates found among the real images. The last row contains synthetic images.

phenomenon causes real images to be more likely to be discarded in later stages (as explained in *food*) and also leads to the loss of relevant images if excessive pruning is carried out.

To conclude, we present in Figure 14 60 random images of PaS-B: 30 real and 30 synthetic. It should be noted that the visual gap between both sets is much smaller than in the case of food.

C Visualization of Conceptual Prototypes

As explained in the main text, we used the tool *ProtoSim* [65] to compare the PaS datasets with their SoTA supervised counterpart. We use the official implementation and the default configuration from [65] for both domains. In Fig. 15, we can see some examples of the most relevant prototypes of each dataset.

C.1 Food Domain

Among the 8192 prototypes, 8144 are shared in both Food-2K [46] and PaS-F. Regarding the exclusive ones (the remaining 48), they are distributed as follows: 16 belong to Food-2K and 32 belong to PaS-F. Even if Food-2K is a human-labelled dataset, it contains several image repetitions that fill its exclusive prototypes. On the contrary, among the PaS-F exclusive prototypes, there are more than 300 unique samples that show a diversity not included in Food-2K.

C.2 Birds Domain

From the 8192 prototypes found by *ProtoSim*, a total of 33 are classified as exclusive. Among those, 10 belong to iNat_{Birds} and 23 to PaS-B. While the

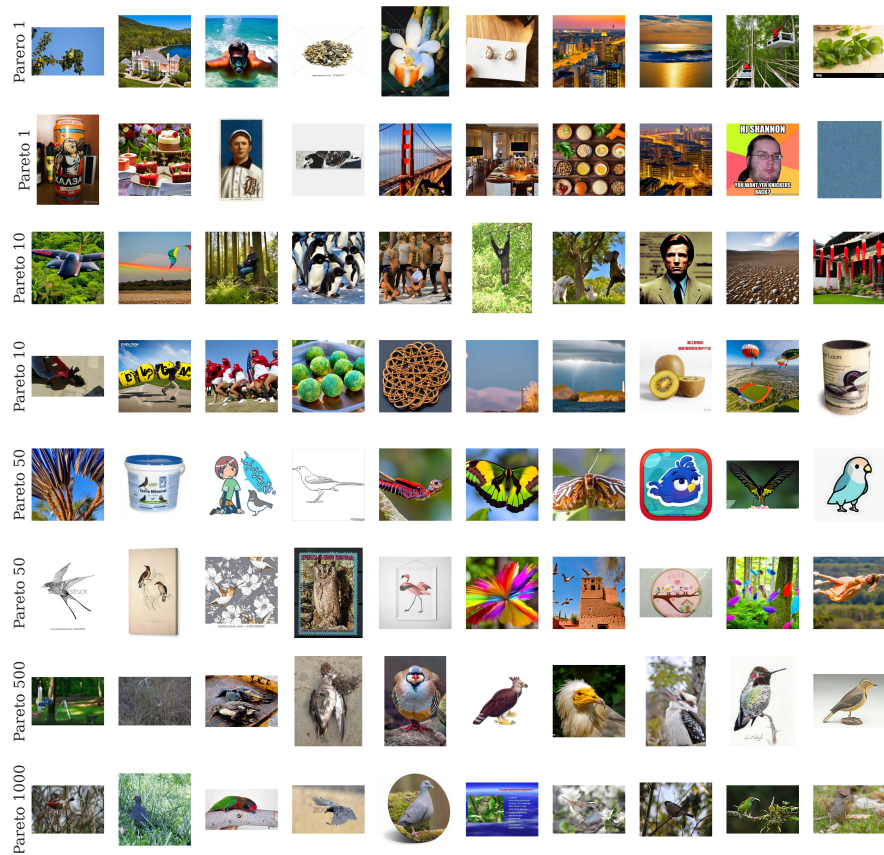


Fig. 13: Examples of images removed during the Pareto-based removal for the *birds* domain. “Pareto n ” refers to images belonging to the n -th Pareto front (removed in the n -th iteration).

sum of all the samples in the $i\text{Nat}_{Birds}$ prototypes is below 30, our exclusive prototype contains more than 350 samples, showing a much higher diversity not only regarding the prototypes but also the population of these prototypes.

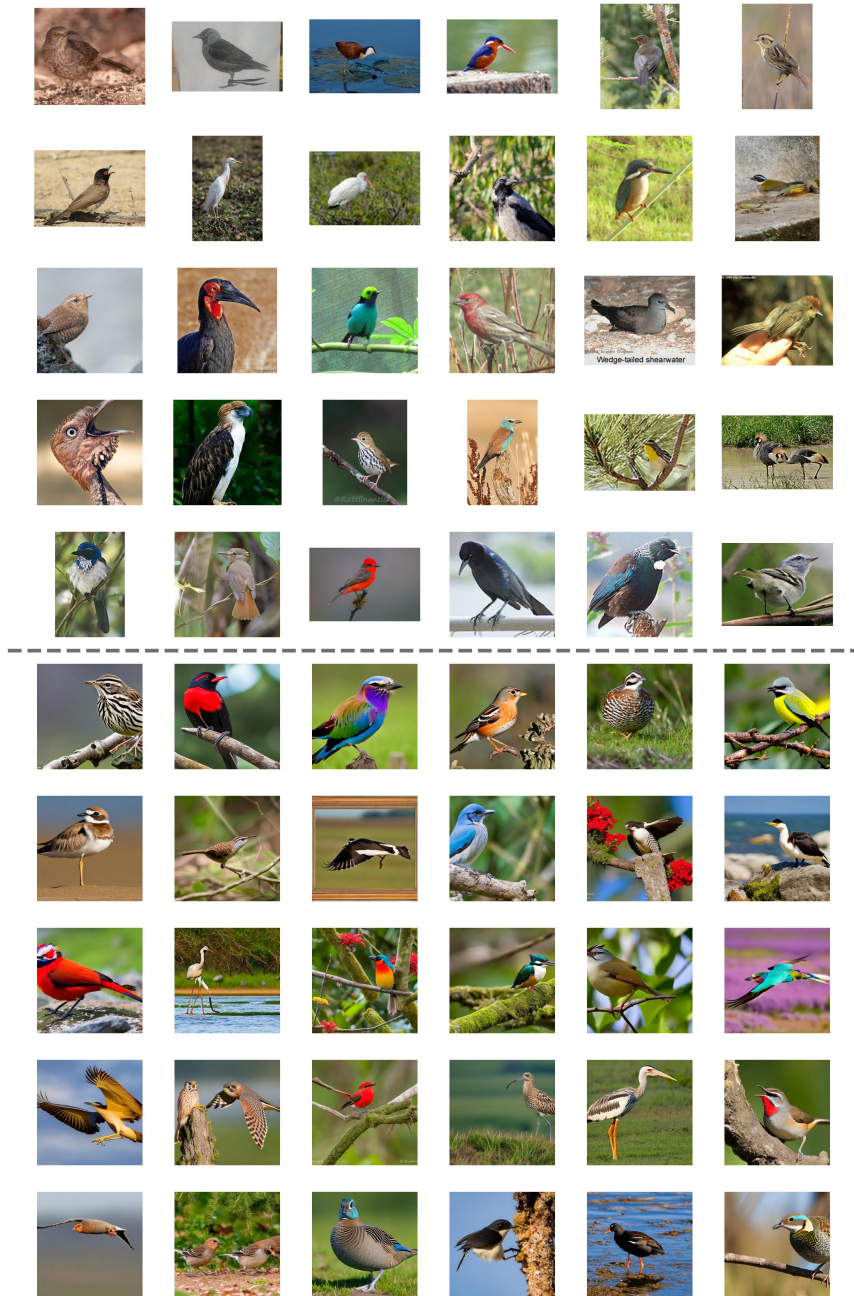


Fig. 14: Examples from PaS-B dataset. The first 5 rows correspond to real images (from LAION-5B). The 5 bottom rows are generated by SD 2.1.

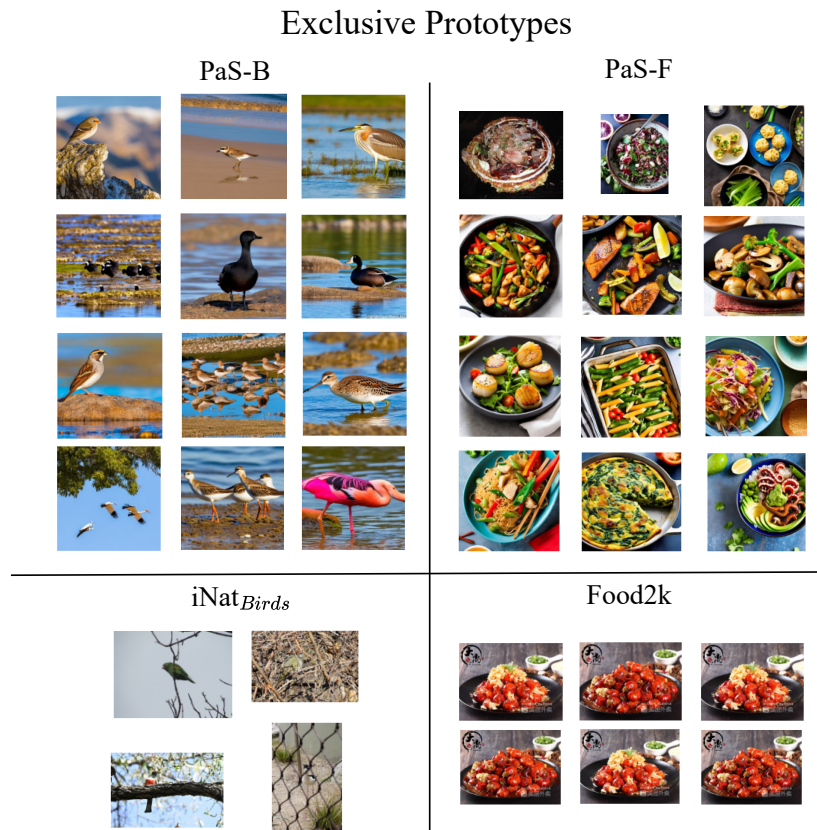


Fig. 15: Examples from the extracted prototypes. All of them belong to an exclusive prototype of their corresponding dataset.

D Experiment Setup

D.1 Dataset Creation

In the main text, we already mentioned the values of the main hyperparameters as well as the main configurations of PaS. In this section, we describe in more detail the implementation and technical aspects of the pipeline tested in this research. Note that container definition files will be made publicly available to reproduce all the environments.

Concept Generation and Expansion. We use Mixtral-8x7B [32] and Llama-2 13B (chat finetuned) [62], both with the weights quantized with the method Q5_K_M^{4,5}. The inference is executed using *LangChain* version *v0.1.3* and the library *llama.cpp* as backend.

Real Image Retrieval. In order to query images from LAION-5B, we rely on the library *clip-retrieval* [5] to build a search index from the CLIP embeddings. For all the datasets, we use CLIP as an encoder. The library already provides a search index for the LAION-5B dataset based on CLIP ViT-L/14. Regarding the retrieval process itself, the same library was used, asking for a maximum of 500 results per query and keeping all the default parameter values from [5].

Synthetic Image Generation. We generate images using the text-to-image method Stable Diffusion 2.1 [54]. Given the large number of images that we need to generate, we resort to *TensorRT* version *8.6* to speedup the inference process⁶.

Image Filtering. For SSCD [52] similarity detection, we use a k-NN algorithm to detect the most similar images to each one. Regarding the **data leak detection**, we use $k = 32$. For the **deduplication** process, we use $k = 64$. For each connected component of duplicates of the associated k-NN graph, one image is selected randomly and the others are removed from the dataset. To make the process faster, we use FAISS [20] for k-NN computation. Regarding the Pareto-front-based filtering, we use the official implementation and weights of CLIPN-CTW⁷ [21] for out-of-distribution detection. For image detection and blurring, we use the same model and settings utilised in [43].

⁴ <https://huggingface.co/TheBloke/Mixtral-8x7B-Instruct-v0.1-GGUF>

⁵ <https://huggingface.co/TheBloke/Llama-2-13B-chat-GGUF>

⁶ <https://github.com/NVIDIA/TensorRT/tree/release/8.6/demo/Diffusion>

⁷ <https://github.com/xmed-lab/CLIPN/>

D.2 Pretraining

To train the backbones used in the experiments shown in the main text and this supplementary material, three kinds of pretraining are considered:

- Supervised pretraining: The ViT-B [60] pretrained with ImageNet-21K [55] was trained in a supervised way using the original labels from the dataset [60]. As the rest of the pretrainings presented, it is done for 300 epochs, but the augmentations used in this case were heavily tuned.
- Self-supervised pretraining using NNCLR [22]: We pretrain the ResNets using NNCLR method. Selected parameters are extracted directly from the original paper [22].
- Self-supervised pretraining using MoCov3 [11]: We decided to pretrain all ViT-B models using MoCov3 as they benefit from the stability provided by the method. All experiments are performed with the parameters stated in the original paper [11].

D.3 Downstream Tasks

All downstream tasks are performed using a single NVIDIA A100 with 40GB of VRAM. These tasks were designed to assess the quality of features learned by the backbones pretrained using different datasets. For the sake of simplicity, we maintain the same hyperparameters across datasets.

Linear Classification. In this downstream task, we freeze the pretrained backbones and add only a linear layer at the end, which is trained to classify elements of the target dataset based on the features produced by the backbone. The number of training epochs is 100 in all the experiments. For the ResNet backbones, we use SGD with a step scheduler with a reduction factor of 10 in the learning rate at epochs 60 and 80. For ViT, we use AdamW with a cosine scheduler.

Finetuning Classification. This downstream task corresponds to the most typical way of transfer learning, in which both the backbone and the classification layer are trained on a different dataset than the pretraining one. The hyperparameters are the same as in linear classification, and the only difference is that the weights of the backbone are updated during the training.

k-Nearest Neighbours (k-NN). This downstream task does not involve additional training. Instead, for every image in the training subset of the target dataset, we calculate and store the corresponding embedding from the pretrained backbone. Subsequently, for each image in the test subset, we also compute its embedding. To make a prediction, we identify the closest embedding from the training subset (utilizing cosine similarity as the distance metrics). The predicted class for the test image is then assigned based on the class of its nearest training image. This method assesses the discriminative power of the pretrained backbone’s embeddings directly, without further modification or training.

Semantic Segmentation. The FoodSeg103 dataset [70], which contains detailed annotations of food images, is employed to assess the effectiveness of our models in delineating and distinguishing different food items within an image. All the experiments are executed using the library *MMSegmentation* [14] v1.2.1. We use the UperNet [72] algorithm to test the generalization ability of the features learned from the generated dataset. As a backbone, we use ViT-B. In all the cases, default configurations provided by the *MMSegmentation* library are used, without any hyper-parameter tuning⁸. Each finetuning experiment was done for 80K training steps (like in the FoodSeg103 paper [70]). We use the mean intersection over union (mIoU), computed as the average of the IoU of the categories of the dataset, and average class accuracy (mAcc) as the **evaluation metrics**.

Object Detection. We use the Oktoberfest dataset [81] for object detection to see if our models can accurately locate and identify different food items. We use *MMDetection* v3.2.0 [9] for this task. We use Cascade-RCNN [7], a well-known and widely adopted benchmark algorithm. Like in the case of semantic segmentation, we use the default configurations⁹ without any hyper-parameter tuning. We use the default 12 epoch scheduler for both methods. We use the COCO-style mean average precision (mAP) [40] as the **evaluation metric**.

⁸ <https://github.com/open-mmlab/msegmentation/tree/v1.2.1/configs>

⁹ <https://github.com/open-mmlab/mmdetection/tree/v3.2.0/configs>